

# An ultra-short polarization beam splitter based on dual-core photonic crystal fiber with surface plasmon resonance effect

Ke Wang,<sup>a,1</sup> Yuwei Qu,<sup>a,1</sup> Jinhui Yuan,<sup>a,b,\*</sup> Shi Qiu,<sup>a</sup> Xian Zhou,<sup>b</sup> Binbin Yan,<sup>a</sup> Qiang Wu,<sup>c,d,\*</sup> Bin Liu,<sup>d</sup> Kuiru Wang,<sup>a</sup> Xinzhu Sang,<sup>a</sup> Chongxiu Yu<sup>a</sup>

<sup>a</sup>State Key Laboratory of Information Photonics and Optical Communications, Beijing University of Posts and Telecommunications, Beijing 100876, China

<sup>b</sup>Research Center for Convergence Networks and Ubiquitous Services, University of Science & Technology Beijing (USTB), Beijing 100083, China

<sup>c</sup>Department of Physics and Electrical Engineering, Northumbria University, Newcastle upon Tyne, NE1 8ST, United Kingdom

<sup>d</sup>Key Laboratory of Nondestructive Test (Ministry of Education), Nanchang Hangkong University, Nanchang 330063, China

**Abstract.** In this paper, an ultra-short polarization beam splitter (PBS) based on dual-core photonic crystal fiber (DC-PCF) with surface plasmon resonance (SPR) effect is proposed. The finite element method is used to investigate the coupling characteristics between the core mode and surface plasmon polariton (SPP) mode. The influences of the PCF structure parameters on the coupling length ( $CL$ ) and coupling length ratio ( $CLR$ ) are also investigated. The normalized output powers of the x-polarization and y-polarization are calculated, and the optimized PBS achieves an ultra-short length of 62.5  $\mu\text{m}$ . The splitting bandwidth of 110 nm (1.51~1.61  $\mu\text{m}$ ) is achieved when the extinction ratio ( $ER$ ) is less than -20 dB. The minimum  $ER$  reaches -71 dB at the wavelength of 1.55  $\mu\text{m}$ . The proposed PBS has an important application in the high-speed optical communication system.

**Keywords:** polarization beam splitter, photonic crystal fiber, surface plasmon resonance, extinction ratio.

<sup>1</sup>These authors contributed equally to this work.

\*yuanjinhui81@bupt.edu.cn; qiang.wu@northumbria.ac.uk

## 1. Introduction

With the rapid development of the communication system, the polarization characteristics of optics have attracted great attention. Because the polarization beam splitter (PBS) can split a beam of light into two polarized beams 1, it has widespread applications in optical communication and sensing systems. The larger refractive index difference between the two polarization beams is the key to achieve the PBS with shorter length and wider bandwidth. However, it is difficult to obtain the larger refractive index difference for the traditional dual-core optical fibers because of their structural symmetry and low birefringence 2. Compared with the traditional optical fibers, photonic crystal fiber (PCF) has unique optical characteristics, such as endlessly single-mode 5,6, high birefringence 7, large mode field area 10, controllable dispersion 11, and high nonlinearity 12. Thus, the PCF can be applied for different devices. For example, the PCF-based PBS with shorter length and wider bandwidth could be -achieved.

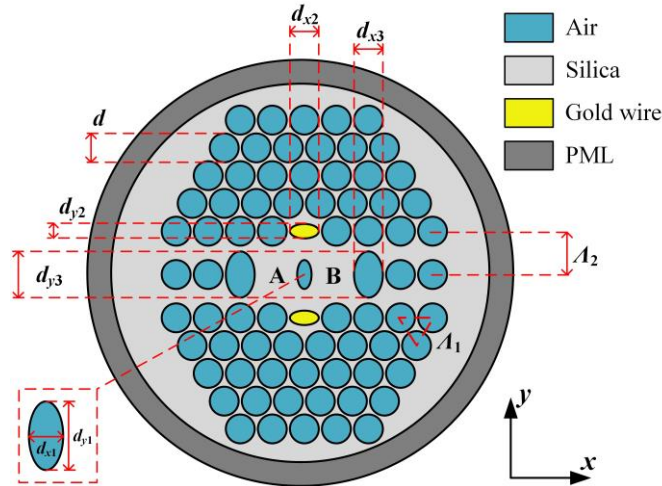
In recent years, some researchers designed different kinds of PBS based on the dual-core PCF (DC-PCF) through breaking the structural symmetry of the DC-PCF, which can be achieved by changing the arrangement of the air holes in the cladding region 19 or introducing the elliptical air holes 19. Moreover, other materials can also be used for replacing the silica substrate and the metal materials can be used for coating or filling the air holes. In 2015, Xu *et al.* reported a DC-PCF PBS with an elliptical hole, which is filled with a kind of low refractive index material. The length and bandwidth of the reported PBS are 401  $\mu\text{m}$  and 140 nm 22. In

43 2016, Wang *et al.* designed a DC-PCF PBS filled with the liquid crystal in the air hole, achieving  
 44 the PBS length of 890.5  $\mu\text{m}$  and bandwidth of 150 nm 23. In 2017, Wang *et al.* proposed a DC-  
 45 PCF PBS with the magnetic fluid added in the air hole, where the PBS length and bandwidth are  
 46 5.1 mm and 189 nm 24. In 2018, Wang *et al.* reported a rectangular-hexagonal structure DC-PCF  
 47 PBS with two elliptical holes in the core region, along with the PBS length of 93.3  $\mu\text{m}$  and  
 48 bandwidth of 40 nm 25. In 2019, Xu *et al.* demonstrated a DC-PCF PBS filled with titanium and  
 49 low refractive index liquid, where the PBS length and bandwidth are 83.9  $\mu\text{m}$  and 32.1 nm 26. In  
 50 2020, Qu *et al.* investigated a gold-coated silicon DC-PCF PBS, where the PBS length and mid-  
 51 infrared bandwidth are 192  $\mu\text{m}$  and 830 nm 27.

52 In this paper, we propose an ultra-short PBS based on the gold-filled DC-PCF. The two cores  
 53 of the DC-PCF are composed by the three elliptical air holes in the horizontal axis. Two elliptical  
 54 gold wires are filled in longitudinal axis to induce the surface plasmon resonance (SPR) effect.  
 55 The PBS can achieve an ultra-short length of 62.5  $\mu\text{m}$  and a bandwidth of 110 nm. The proposed  
 56 DC-PCF PBS has an important application in the high-speed optical communication system.

## 57 2. Design of the DC-PCF PBS and theory

58 The cross-section of the proposed DC-PCF PBS is shown in Fig. 1. The diameter of all circular  
 59 air holes arranged in the triangular array is  $d$ , and the hole-to-hole pitch is  $A_1$ . In addition, the  
 60 three layers of air holes are arranged in a rectangular array in the horizontal direction, and the  
 61 hole-to-hole pitch is  $A_2$ . The air hole in the most center is replaced with an elliptical hole, whose  
 62 minor and major axes are denoted by  $d_{x1}$  and  $d_{y1}$ , respectively. And the two air holes are missing  
 63 on the left and right sides of the central elliptical air hole to form the cores A and B, respectively.  
 64 The air holes on the upper and lower sides of the central elliptical hole are filled by the two  
 65 elliptical gold wires, whose minor and major axes are denoted by  $d_{y2}$  and  $d_{x2}$ , respectively.  
 66 Compared with other metal materials, the gold material has stable chemical property, good  
 67 biomolecular compatibility, and strong corrosion resistance. The left side of the core A and right  
 68 side of the core B are replaced by the two large elliptical air holes, whose minor and major axes  
 69 are denoted by  $d_{x3}$  and  $d_{y3}$ , respectively.



70  
71 **Fig. 1.** The cross-section of the proposed DC-PCF PBS.

72 The background material is the pure silica. The perfect matching layer (PML) of the  
 73 proposed DC-PCF is set at the outermost layer to absorb the radiation energy 28. The inner  
 74 diameter and thickness of the PML are 6  $\mu\text{m}$  and 1.2  $\mu\text{m}$ , respectively. The material of the PML

75 is highly doped silica, and the corresponding refractive index is  $n_{\text{silica}}+0.03$ . The material  
 76 dispersions of the silica and doped silica can be described by the Sellmeier equation [29, 30].  
 77 The dielectric constant of the gold material can be described by the Drude-Lorentz 31

$$\varepsilon_m = \varepsilon_\infty - \frac{\omega_D^2}{\omega(\omega + j\gamma_D)} - \frac{\Delta\varepsilon \cdot \Omega_L^2}{(\omega^2 - \Omega_L^2) - j\Gamma_L\omega}, \quad (1)$$

78 where  $\varepsilon_m$  represents the dielectric constant of gold,  $\varepsilon_\infty = 5.9673$  is the high frequency dielectric  
 79 constant,  $\Delta\varepsilon = 1.09$  is the wave vector,  $\omega$  is the angular frequency of the light, and  $\omega_D$  and  $\gamma_D$  are  
 80 the plasma frequency and Damping frequency, respectively. Here,  $\omega_D/2\pi = 2113.6$  THz, and  
 81  $\gamma_D/2\pi = 15.92$  THz.  $\Omega_L$  and  $\Gamma_L$  are the frequency and spectral width of the Lorentz oscillation,  
 82 respectively.  $\Omega_L/2\pi = 650.07$  THz, and  $\Gamma_L/2\pi = 104.86$  THz.

83 The coupling length ( $CL$ ) of the DC-PCF, where the light power is completely transferred  
 84 from one core to the other one, can be calculated by 32

$$CL_{x,y} = \frac{\lambda}{2(n_{x,y}^{\text{even}} - n_{x,y}^{\text{odd}})}, \quad (2)$$

85 where the  $CL_{x,y}$  is the  $CL$  of the  $x$ -pol and  $y$ -pol,  $\lambda$  is the wavelength of the incident light, and  $n$  is  
 86 the effective refractive indices of the even and odd modes. In order to achieve the complete beam  
 87 splitting, the  $CL$  of the two polarization states needs to satisfy the condition that  $mCL_x = nCL_y =$   
 88  $L$  ( $m$  and  $n$  are the positive integers and  $L$  is the length of the PBS), and the coupling length ratio  
 89 ( $CLR$ ) can be calculated by

$$CLR = \frac{CL_y}{CL_x}, \quad (3)$$

90 When the  $CLR$  reaches 2 or 0.5, the splitting length is the optimum value. The transmission  
 91 loss of the ultra-short PBS is also negligible. Therefore, when the input power  $P_{\text{in}}$  is determined,  
 92 the normalized output power  $P_{\text{out}}$  can be calculated by 33

$$P_{\text{out}}^{x,y} = P_{\text{in}}^{x,y} \cos^2\left(\frac{\pi L}{2CL_{x,y}}\right), \quad (4)$$

93 The performance of the PBS can be described by the extinction ratio ( $ER$ ) as following 34

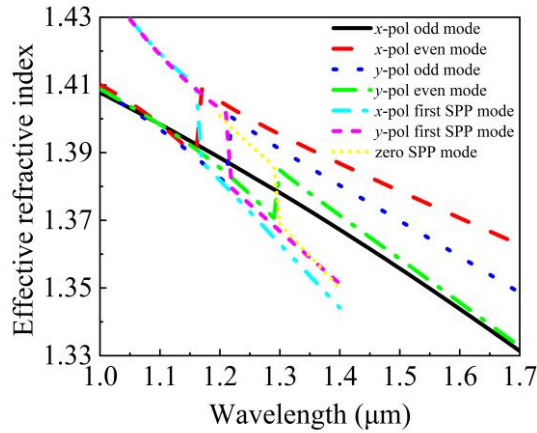
$$ER = 10 \cdot \lg\left(\frac{P_{\text{out}}^y}{P_{\text{out}}^x}\right), \quad (5)$$

94 when the  $ER$  is larger than 20 dB, the propagated light could be completely split, so the  $ER$   
 95 can determine the bandwidth of the PBS.

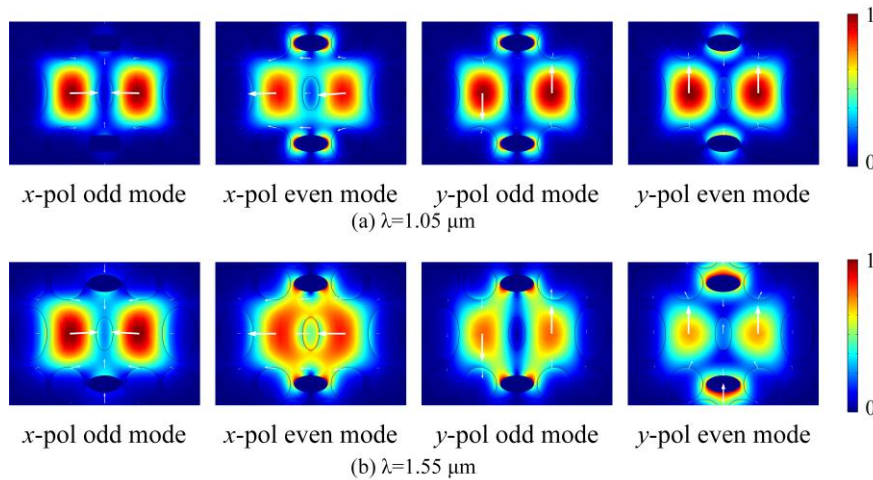
### 96 3. Simulation results and discussion

97 The finite element method (FEM) is adopted to simulate the proposed DC-PCF PBS. Fig. 2  
 98 shows the calculated effective refractive indices of the  $x$ -pol odd and even modes,  $y$ -pol odd and  
 99 even modes,  $x$ -pol and  $y$ -pol first SPP modes, and zero SPP mode. From Fig. 2, the  $x$ -pol even  
 100 mode and  $x$ -pol first SPP mode have a resonance point at wavelength 1.17  $\mu\text{m}$ , the  $y$ -pol odd  
 101 mode and  $y$ -pol first SPP mode have a resonance point at wavelength 1.22  $\mu\text{m}$ , and the  $y$ -pol

102 even mode and zero SPP mode have a resonance point at wavelength  $1.3 \mu\text{m}$ , while there is no  
 103 resonance point between the  $x$ -pol odd mode and SPP mode. According to the coupling mode  
 104 theory 35, the  $x$ -pol even,  $y$ -pol odd, and  $y$ -pol even modes are completely coupled with the  $x$ -pol  
 105 first SPP,  $y$ -pol first SPP, and zero SPP modes, respectively. In order to further verify the above  
 106 conclusions, the mode field distributions of the  $x$ -pol and  $y$ -pol even and odd modes at  
 107 wavelengths  $1.05 \mu\text{m}$  and  $1.55 \mu\text{m}$  are shown in Figs. 3(a) and 3(b), respectively. From Fig. 3(a),  
 108 the mode field energies of the  $x$ -pol and  $y$ -pol odd and even modes do not occur to change at  
 109 wavelength  $1.05 \mu\text{m}$ , which indicate that before wavelength  $1.05 \mu\text{m}$ , there are no mode coupling  
 110 between the considered modes and SPP modes. From Fig. 3(b), the mode field energy of the  $x$ -  
 111 pol odd mode does not occur to change, and the mode field energies of the  $x$ -pol even,  $y$ -pol odd,  
 112 and  $y$ -pol even modes occur to transfer. It indicates that the  $x$ -pol even,  $y$ -pol odd, and  $y$ -pol even  
 113 modes occur to couple with the  $x$ -pol first SPP mode,  $y$ -pol first SPP mode, and zero SPP mode,  
 114 respectively, after  $1.55 \mu\text{m}$ . Because the coupling strengths based on the SPR effect for different  
 115 modes are different, the effective refractive index differences between the  $x$ -pol and  $y$ -pol modes  
 116 are increased, and the DC-PCF PBS could be achieved due to the enhanced birefringence.

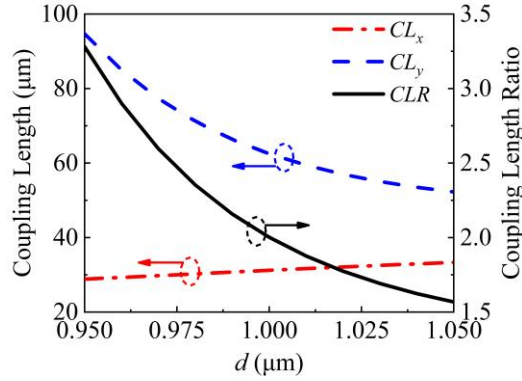


117  
 118 **Fig. 2.** The effective refractive indices of the  $x$ -pol odd and even modes,  $y$ -pol odd and even modes,  $x$ -pol and  $y$ -pol  
 119 first SPP modes, and zero SPP mode calculated as functions of wavelength.



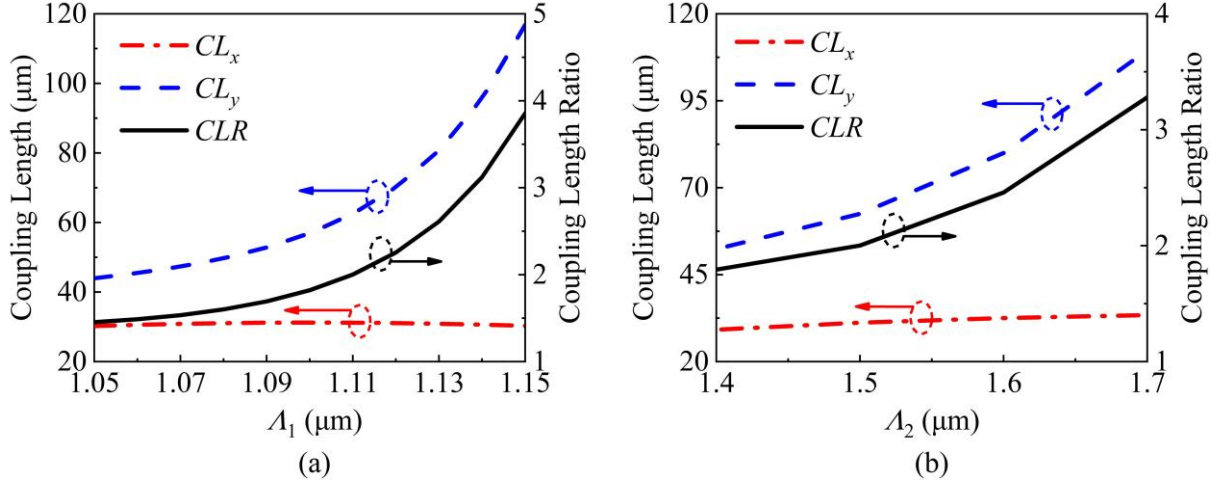
120  
 121 **Fig. 3.** The mode field distributions of the  $x$ -pol odd mode,  $x$ -pol even mode,  $y$ -pol odd mode, and  $y$ -pol even mode  
 122 calculated at wavelengths (a)  $1.05 \mu\text{m}$  and (b)  $1.55 \mu\text{m}$ .

123 In the following, the structure parameters, including  $d$ ,  $A_1$ ,  $A_2$ ,  $d_{x1}$ ,  $d_{y1}$ ,  $d_{y2}$ ,  $d_{x2}$ ,  $d_{x3}$ , and  $d_{y3}$ ,  
 124 are, respectively, adjusted at wavelength 1.55  $\mu\text{m}$  to optimize the performance of the DC-PCF  
 125 PBS. The relationships between the  $CL_x$ ,  $CL_y$ , and  $CLR$  and  $d$  are shown in Fig. 4. When  $d$   
 126 changes from 0.95 to 1.05  $\mu\text{m}$ , the effective refractive indices of the  $x$ -pol odd and even modes  
 127 decrease, but the decrease amplitude of the  $x$ -pol even mode is larger than that of the  $x$ -pol odd  
 128 mode. Meanwhile, the effective refractive indices of the  $y$ -pol odd and even modes also decrease,  
 129 but the decrease amplitude of the  $y$ -pol even mode is larger than that of the  $y$ -pol odd mode. Thus,  
 130 the effective refractive index differences between the  $x$ -pol odd and even modes and  $y$ -pol odd  
 131 and even modes become smaller. As shown in Fig. 4, the  $CL_x$  increases from 28 to 33  $\mu\text{m}$ , and  
 132 the  $CL_y$  decreases from 92 to 52  $\mu\text{m}$ . It can be deduced from Eq. (3) that the  $CLR$  decreases from  
 133 3.2 to 1.5  $\mu\text{m}$ . When  $d=1 \mu\text{m}$ , the  $CLR=2.048$ , which is very close to the ideal value of 2.



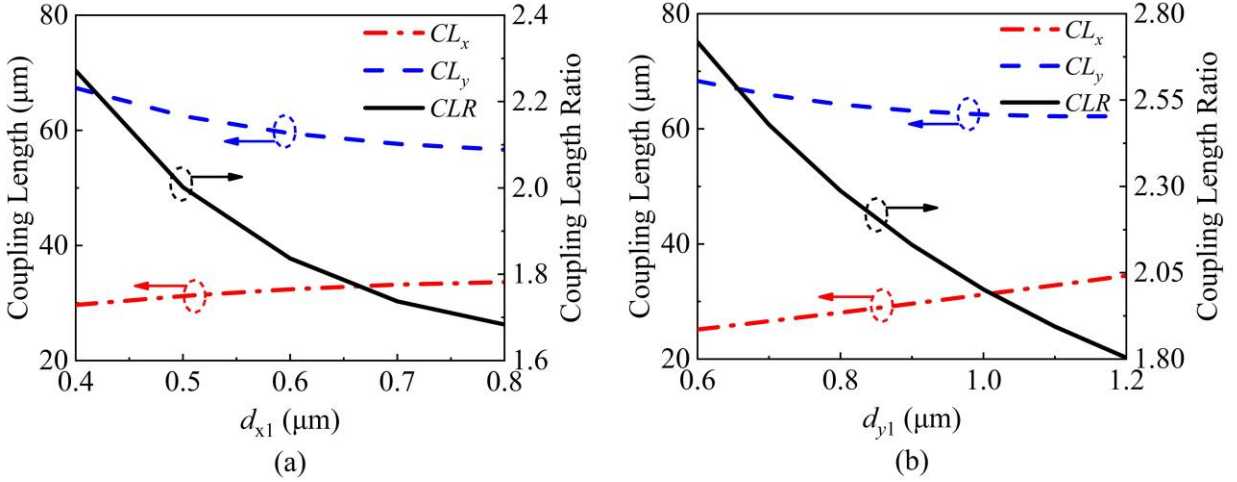
134  
 135 **Fig. 4.** The relationships between the  $CL_x$ ,  $CL_y$ , and  $CLR$  and  $d$ .

136 When  $A_1$  changes from 1.05 to 1.15  $\mu\text{m}$ , the effective refractive indices of the  $x$ -pol odd and  
 137 even modes increase, and the increase amplitude of the  $x$ -pol even mode is approximately equal  
 138 to that of the  $x$ -pol odd mode. Although the effective refractive indices of the  $y$ -pol odd and even  
 139 modes also increase, the increase amplitude of the  $y$ -pol even mode is larger than that of the  $y$ -  
 140 pol odd mode. Thus, the effective refractive index difference between the  $x$ -pol odd and even  
 141 modes remains almost unchanged, while the effective refractive index difference between the  $y$ -  
 142 pol odd and even modes becomes smaller. As shown in Fig. 5(a), the  $CL_x$  is stabilized at 30  $\mu\text{m}$ ,  
 143 and the  $CL_y$  increases from 43 to 120  $\mu\text{m}$ . According to Eq. (3), the  $CLR$  increases from 1.4 to  
 144 3.8  $\mu\text{m}$ . When  $A_1=1.11 \mu\text{m}$ , the  $CLR$  is very close to 2. From Fig. 5(b), when  $A_2$  changes from 1.4  
 145 to 1.7  $\mu\text{m}$ , the  $CL_x$  increases from 29 to 33  $\mu\text{m}$ , the  $CL_y$  increases from 52 to 109  $\mu\text{m}$ , and the  
 146 corresponding  $CLR$  increases from 1.79 to 3.2. When  $A_2=1.6 \mu\text{m}$ , the  $CLR$  is very close to 2.



147  
148

**Fig. 5.** The relationships between the  $CL_x$ ,  $CL_y$ , and  $CLR$  and (a)  $A_1$  and (b)  $A_2$ .

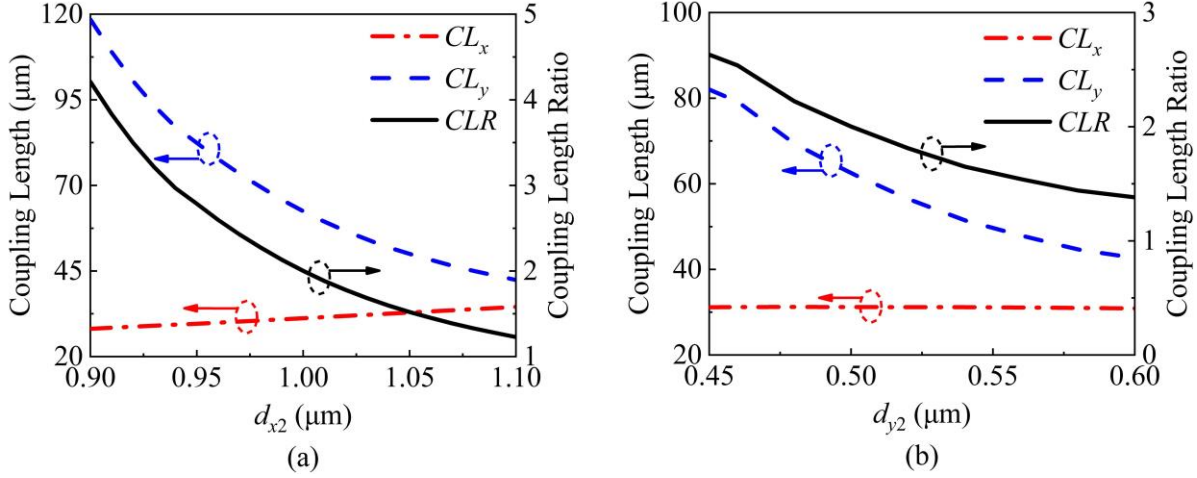


149  
150

**Fig. 6.** The relationships between the  $CL_x$ ,  $CL_y$ , and  $CLR$  and (a)  $d_{x1}$  and (b)  $d_{y1}$ .

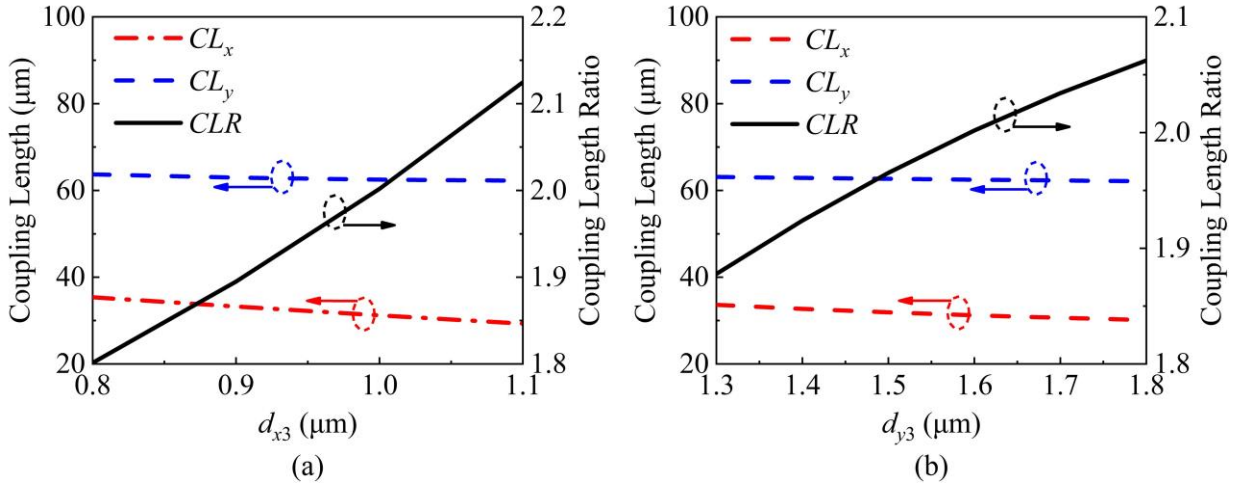
151 The influences of the elliptical hole sizes are shown in Figs. 6(a) and 6(b). When  $d_{x1}$  changes  
 152 from 0.4 to 0.8  $\mu\text{m}$ , the effective refractive indices of the  $x$ -pol odd and even modes decrease, but  
 153 the decrease amplitude of the  $x$ -even mode is larger than that of the  $x$ -odd mode. Although the  
 154 effective refractive index of the  $y$ -pol odd mode remains almost unchanged, the effective  
 155 refractive index of the  $y$ -pol even mode gradually decreases. Thus, the effective refractive index  
 156 difference between the  $x$ -pol odd and even modes becomes smaller, and the effective refractive  
 157 index difference between the  $y$ -pol odd and even modes becomes larger. As shown in Fig. 6(a),  
 158 the  $CL_x$  increases from 29 to 33  $\mu\text{m}$ , the  $CL_y$  decreases from 67 to 56  $\mu\text{m}$ , and the corresponding  
 159  $CLR$  decreases from 2.2 to 1.6. When  $d_{x1}=0.5$   $\mu\text{m}$ , the  $CLR$  is very close to 2. When  $d_{y1}$  increases  
 160 from 0.6 to 1.2, the effective refractive index difference of the  $x$ -pol odd and even modes  
 161 becomes smaller, and the effective refractive index difference between the  $y$ -pol odd and even  
 162 modes also becomes larger. As shown in Fig. 6(b), the  $CL_x$  increases from 25 to 34  $\mu\text{m}$ , the  $CL_y$   
 163 decreases from 68 to 62  $\mu\text{m}$ , and the corresponding  $CLR$  decreases from 2.7 to 1.8. When  $d_{y1}=1$   
 164  $\mu\text{m}$ , the  $CLR$  is very close to 2.





165  
166 **Fig. 7.** The relationships between the  $CL_x$ ,  $CL_y$ , and  $CLR$  and (a)  $d_{x2}$  and (b)  $d_{y2}$ .

167 The influences of the elliptical gold wires are shown in Figs. 7(a) and 7(b). When  $d_{x2}$   
168 changes from 0.9 to 1.1 μm, the effective refractive index of the  $x$ -pol odd mode remains almost  
169 unchanged, but the effective refractive index of the  $x$ -pol even mode gradually decreases.  
170 Although the effective refractive indices of the  $y$ -pol odd and  $y$ -pol even modes decrease, the  
171 decrease amplitude of the  $y$ -pol even mode is larger than that of the  $y$ -pol odd mode. Thus, the  
172 effective refractive index difference between the  $x$ -pol odd and  $x$ -pol even modes becomes  
173 smaller, and the effective refractive index difference between the  $y$ -pol odd and  $y$ -pol even  
174 modes becomes larger. As shown in Fig. 7(a), the  $CL_x$  increases from 28 to 34 μm, the  $CL_y$   
175 decreases from 118 to 42 μm, and the corresponding  $CLR$  decreases from 4.2 to 1.2. When  $d_{x2}=1$   
176 μm, the  $CLR=2$ . When  $d_{y2}$  increases from 0.45 to 0.6, the effective refractive index difference  
177 between the  $x$ -pol odd and  $x$ -pol even modes remains almost unchanged, and the effective  
178 refractive index difference between the  $y$ -pol odd and  $y$ -pol even modes becomes larger. As  
179 shown in Fig. 7(b), the  $CL_x$  is stabilized at 30 μm, the  $CL_y$  decreases from 131 to 42 μm, and  
180 the corresponding  $CLR$  decreases from 4.2 to 1.38. When  $d_{y2}=0.5$  μm, the  $CLR$  is very close to 2.

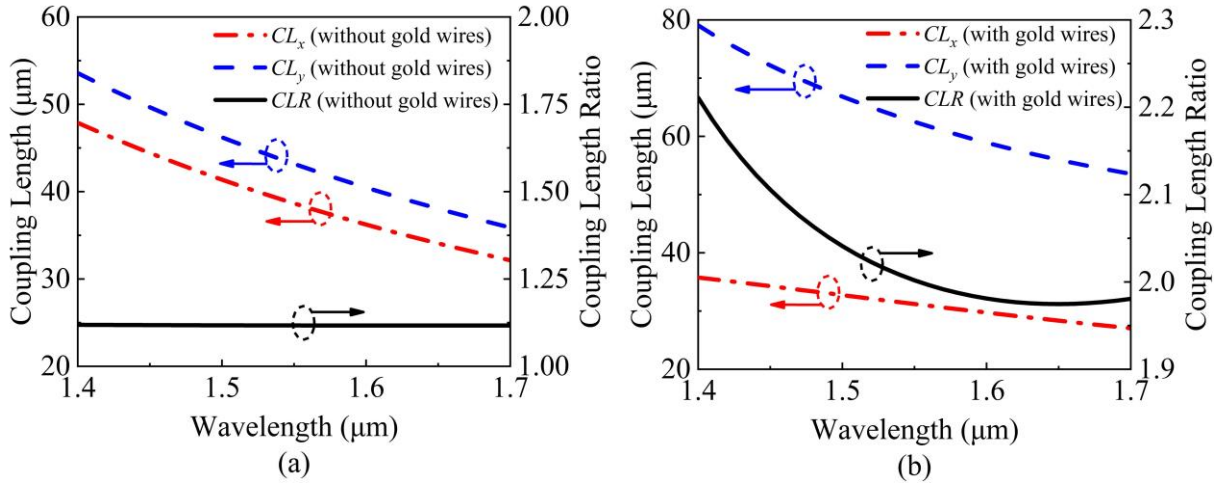


181  
182 **Fig. 8.** The relationships between the  $CL_x$ ,  $CL_y$ , and  $CLR$  and (a)  $d_{x3}$  and (b)  $d_{y3}$ .

183 The influences of the large elliptical air hole along the horizontal axis are shown in Figs. 8(a)  
184 and 8(b). When  $d_{x3}$  changes from 0.8 to 1.1 μm, the effective refractive index of the  $x$ -pol odd

185 mode decreases slightly, and the effective refractive index of the  $x$ -pol even mode remains  
 186 almost unchanged. Meanwhile, the effective refractive indices of the  $y$ -pol odd and  $y$ -pol even  
 187 modes remain almost unchanged. Thus, the effective refractive index difference between the  $x$ -  
 188 pol odd and  $x$ -pol even modes becomes larger, and the effective refractive index differences  
 189 between the  $y$ -pol odd and  $y$ -pol even modes changes slightly. From Fig. 8(a), as the  $CL_x$   
 190 decreases, the  $CL_y$  is almost constant, and the corresponding  $CLR$  increases. As  $d_{y3}$  increases  
 191 from 1.3 to 1.8, the effective refractive indices of the  $x$ -pol odd and  $x$ -pol even modes and  $y$ -pol  
 192 odd and  $y$ -pol even modes decrease, and the decrease amplitudes of the  $x$ -pol odd and  $y$ -pol odd  
 193 modes are approximately equal to those of the  $x$ -pol even and  $y$ -pol even modes. It can be seen  
 194 from Fig. 8(b) that the  $CL_x$  and  $CL_y$  are almost constant, but the corresponding  $CLR$  increases.

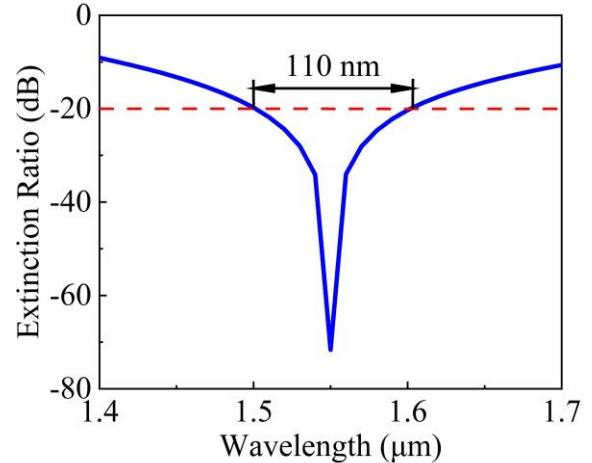
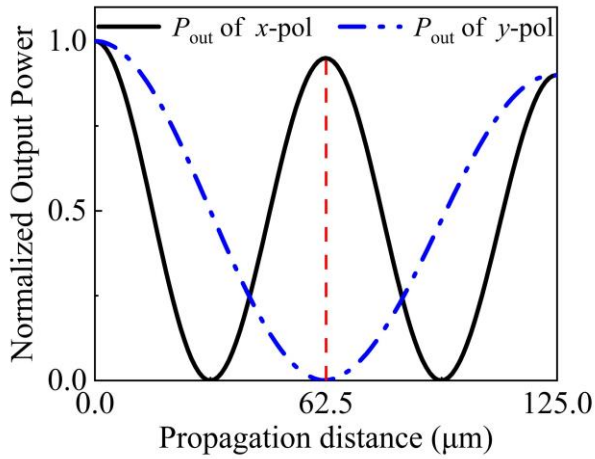
195 As shown in Fig. 9(a), when the gold wire is not filled in the two elliptical air holes, the  
 196  $CLR$  can only maintain at 1.1 in the wavelength range from 1.4 to 1.7  $\mu\text{m}$ . At this time, it is  
 197 difficult to completely split the polarized light between the two cores. As shown in Fig. 9(b),  
 198 when the two elliptical air holes are filled with the gold wires, the  $CLR$  decreases from 2.21 to  
 199 1.98 in the considered wavelength range, and reaches 2 at wavelength 1.55  $\mu\text{m}$ . Therefore, the  
 200 gold wire plays an important role in achieving the PBS.  
 201



202  
 203 **Fig. 9.** The relationships between the  $CL$  and  $CLR$  and wavelength, (a) without gold wires, and (b) with gold wires.

204 In summary, the optimized structure parameters of the DC-PCF PBS are chosen as  
 205 following:  $A_1=1.11 \mu\text{m}$ ,  $A_2=1.5 \mu\text{m}$ ,  $d=1 \mu\text{m}$ ,  $d_{x1}=0.5 \mu\text{m}$ ,  $d_{y1}=1 \mu\text{m}$ ,  $d_{x2}=1 \mu\text{m}$ ,  $d_{y2}=0.5 \mu\text{m}$ ,  $d_{x3}=1$   
 206  $\mu\text{m}$ , and  $d_{y3}=1.6 \mu\text{m}$ . Fig. 10(a) shows the relationship between  $P_{\text{out}}$  of  $x$ -pol and  $y$ -pol and  
 207 propagation distance. As shown in Fig. 10(a), when the light at wavelength 1.55  $\mu\text{m}$  enters the  
 208 core A,  $P_{\text{out}}$  of the  $x$ -pol and  $y$ -pol will periodically change with the propagation distance. When  
 209 the propagation distance is 62.5  $\mu\text{m}$ ,  $P_{\text{out}}$  of the  $x$ -pol reaches the maximum value, and  $P_{\text{out}}$  of the  
 210  $y$ -pol is close to 0. At this time, the two polarization states can be completely separated. For the  
 211 core B, the case is exactly opposite. Due to the ohmic loss of metal, the maximum value of the  
 212 normalized power will decrease with the propagation distance 36. Thus, the optimal DC-PCF  
 213 PBS length is 62.5  $\mu\text{m}$ . Fig. 10(b) shows the relationship between the  $ER$  and wavelength when  
 214 the DC-PCF PBS length is 62.5  $\mu\text{m}$ . It can be seen from Fig. 10(b) that the  $ER$  reaches the  
 215 maximum value of -71 dB at wavelength 1.55  $\mu\text{m}$ , and is less than -20 dB in the wavelength  
 216 range of 1.5 to 1.61  $\mu\text{m}$ . The bandwidth of the DC-PCF PBS is 110 nm, covering the whole C  
 217 band.





218  
219  
220

**Fig. 10.** (a) The relationship between  $P_{out}$  of the  $x$ -pol and  $y$ -pol and propagation distance, and (b) the relationship between the  $ER$  and wavelength.

221

Table 1. The comparisons between other proposed PCF PBSs and this work.

Reference	PBS length	Bandwidth	$ER$ at 1550 nm
22	1.890 mm	9 nm	-83.2 dB
23	0.175 mm	250 nm	-80.7 dB
25	1.0 mm	280 nm	-83.6 dB
26	1.746 mm	47 nm	-60 dB
<b>Error! Reference source not found.</b>	830 $\mu$ m	20 nm	-60 dB
[42]	254.6 $\mu$ m	560 nm	-111 dB
This work	62.5 $\mu$ m	110 nm	-71 dB

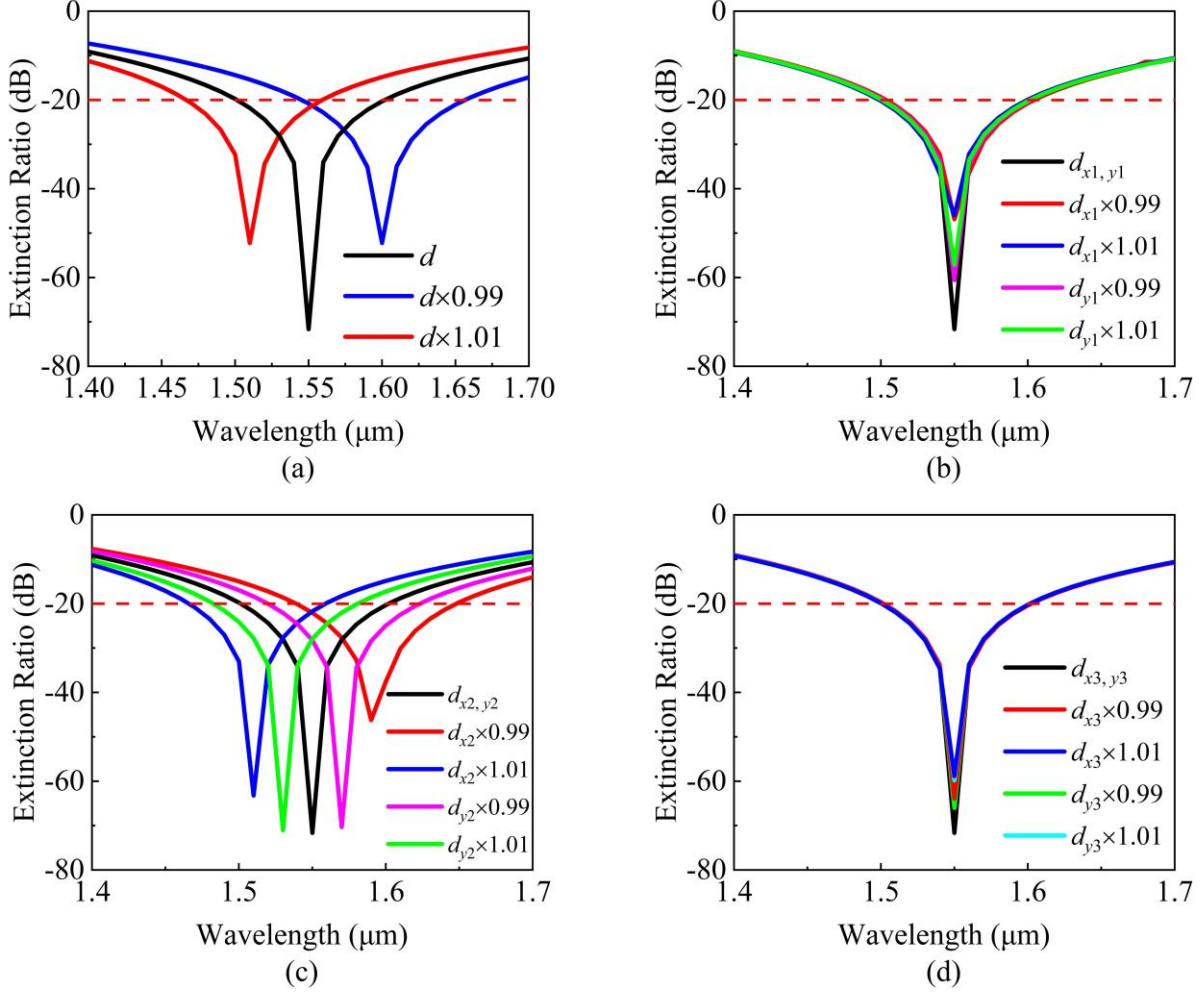


**Fig. 11.** The relationships between the *ER* and wavelength under  $\pm 1\%$  error of (a)  $d$ , (b)  $d_{x1}$ ,  $d_{y1}$  (c)  $d_{x2}$ ,  $d_{y2}$ , and (d)  $d_{x3}$ ,  $d_{y3}$ .

222  
223  
224  
225  
226  
227  
228  
229  
230  
231  
232  
233  
234  
235  
236  
237  
238  
239

Table 1 shows the comparisons between other proposed PCF PBSs and this work [37-42]. It can be concluded from Table 1 that although the bandwidths of the PBSs proposed in Refs [38, 39, 42] are slightly wider than that of this work, the DC-PCF PBS proposed in this work has the shortest length. This is more conducive to the development of photonic integration. Moreover, the bandwidth and *ER* are also good. Finally, we will consider the fabrication tolerance of the proposed DC-PCF PBS. We investigated the dependence of the *ER* on each structure parameter under the fabrication tolerance of 1%. As shown in Fig. 11(a), when  $d$  is reduced or increased by 1%, the bandwidth is red-shifted to 1.54 - 1.64  $\mu\text{m}$  or blue-shifted to 1.46 - 1.56  $\mu\text{m}$ . The DC-PCF PBS can still work well. As shown in Figs. 11(b) and 11(d), when  $d_{x1}$  and  $d_{y1}$ , and  $d_{x3}$  and  $d_{y3}$  are reduced or increased by 1%, only the *ER* at wavelength 1.55  $\mu\text{m}$  is changed, and the bandwidth of the proposed DC-PCF PBS does not change. As shown in Fig. 11(c). when  $d_{x2}$  and  $d_{y2}$  are reduced by 1%, the bandwidth is blue-shifted to 1.53 - 1.65  $\mu\text{m}$  and 1.51 - 1.63  $\mu\text{m}$ , respectively. When  $d_{x2}$  and  $d_{y2}$  are increased by 1%, the bandwidth is red-shifted to 1.43- 1.57  $\mu\text{m}$  and 1.41- 1.57  $\mu\text{m}$ , respectively. Therefore, the proposed DC-PCF PBS has good fabrication tolerance.

#### 240 4. Conclusion

241 In conclusion, we design an ultra-short DC-PCF PBS based on the SPR effect. The performance  
242 of the proposed DC-PCF PBS is optimized through adjusting structure parameters. The *CLR* at  
243 wavelength 1.55  $\mu\text{m}$  is very close to 2. The optimized DC-PCF PBS length is 62.5  $\mu\text{m}$ , the *ER* at  
244 wavelength 1.55  $\mu\text{m}$  is -68.76 dB, and the bandwidth is 110 nm (1.5 - 1.61  $\mu\text{m}$ ), which can cover  
245 the whole C band. The proposed DC-PCF PBS has ultra-short length, large bandwidth, and high  
246 *ER*, and can find important application in the micro-optical system.

#### 247 Disclosures

248 The authors declare no conflicts of interest.

#### 249 Acknowledgement

250 This work is supported by National Key Research and Development Project of China  
251 (2019YFB2204001).

#### 252 References

- 253 1.W. L. Lu, S. Q. Lou, X. Wang, et al. "Ultrabroadband polarization splitter based on three-core photonic  
254 crystal fibers," *Appl. Opt.* **52**(3), 449-455 (2013).
- 255 2.A. N. Miliou, R. Srivastava, R. V. Ramaswamy. "A 1.3- $\mu\text{m}$  directional coupler polarization splitter by  
256 ion exchange," *J. Lightw. Technol.* **11**(2), 220-225 (1993).
- 257 3.G. D. Peng, T. Tjugiarto, P. L. Chu. "Polarisation beam splitting using twin-elliptic-core optical fibres,"  
258 *Electron. Lett.* **26**(10), 682-683 (1990).
- 259 4.C. W. Wu, T. L. Wu, H. C. Chang. "A novel fabrication method for all-fiber, weakly fused, polarization  
260 beamsplitters," *IEEE Photon. Technol. Lett.* **7**(7), 786-788 (1995).
- 261 5.T. A. Birks, J. C. Knight, P. S. J. Russell. "Endlessly single-mode photonic crystal fiber," *Opt. Lett.*  
262 **22**(13), 961-963 (1997).
- 263 6.J. C. Knight, T. A. Birks, R. F. Cregan, et al. "Large mode area photonic crystal fibre," *Electron. Lett.*  
264 **34**(13), 1347-1348 (1998).
- 265 7.A. Ortigosa-Blanch, J. C. Knight, W. J. Wadsworth, et al. "Highly birefringent photonic crystal fibers,"  
266 *Opt. Lett.* **25**(18), 1325-1327 (2000).
- 267 8.M. J. Steel, R. M. Osgood. "Polarization and dispersive properties of elliptical-hole photonic crystal  
268 fibers," *J. Lightw. Technol.* **19**(4), 495 (2001).
- 269 9.T. P. Hansen, J. Broeng, S. E. B. Libori, et al. "Highly birefringent index-guiding photonic crystal  
270 fibers," *IEEE Photon. Technol. Lett.* **13**(6), 588-590 (2001).
- 271 10.Q. Liu, S. G. Li, Z. K. Fan, et al. "Numerical analysis of ultrabroadband polarization splitter based on  
272 gold-filled dual-core photonic crystal fiber," *Opt. Commun.* **334**, 46-50 (2015).
- 273 11.S. Kim, C. S. Kee. "Dispersion properties of dual-core photonic-quasicrystal fiber," *Opt. Express*  
274 **17**(18), 15885-15890 (2009).
- 275 12.X. Li, Z. Xu, W. Ling, et al. "Design of highly nonlinear photonic crystal fibers with flattened  
276 chromatic dispersion," *Appl. Opt.* **53**(29), 6682-6687 (2014).
- 277 13.L. Zhang, C. Yang. "Polarization splitter based on photonic crystal fibers," *Opt. Express* **11**(9), 1015-  
278 1020 (2003).
- 279 14.M. F. O. Hameed, S. S. A. Obayya. "Polarization splitter based on soft glass nematic liquid crystal  
280 photonic crystal fiber," *IEEE Photon. J.* **1**(6), 265-276 (2009).
- 281 15.M. Y. Chen, B. Sun, Y. K. Zhang, et al. "Design of broadband polarization splitter based on partial  
282 coupling in square-lattice photonic-crystal fiber," *Appl. Opt.* **49**(16), 3042-3048 (2010).
- 283 16.L. Jiang, Y. Zheng, L. Hou, et al. "An ultrabroadband polarization splitter based on square-lattice  
284 dual-core photonic crystal fiber with a gold wires," *Opt. Commun.* **351**, 50-56 (2015).

285 17.C. Dou, X. Jing, S. Li, et al. "A compact and low-loss polarization splitter based on dual-core photonic  
286 crystal fiber," *Opt. Quant. Electron.* **50**(6), 255 (2018).

287 18.X. Wang, S. Li, H. Chen, et al. "Polarization splitter based on dual-core photonic crystal fiber with  
288 octagonal lattice," *Opt. Quant. Electron.* **48**(4), 271 (2016).

289 19.N. Florous, K. Saitoh, M. Koshiba. "A novel approach for designing photonic crystal fiber splitters  
290 with polarization-independent propagation characteristics," *Opt. Express* **13**(19), 7365-7373 (2005).

291 20.D. Rajeswari, A. S. Raja, S. Selvendran. "Design and analysis of polarization splitter based on dual-  
292 core photonic crystal fiber," *Optik.* **144**, 15-21 (2017).

293 21.F. He, W. Shi, Z. Hui, et al. A dual-core PCF polarization splitter with five elliptical air holes based on  
294 tellurite glass," *Opt. Quant. Electron.* **49**(11), 363 (2017).

295 22.Z. Xu, X. Li, W. Ling, et al. "Design of short polarization splitter based on dual-core photonic crystal  
296 fiber with ultra-high extinction ratio," *Opt. Commun.* **354**, 314-320 (2015).

297 23.E. L. Wang, H. M. Jiang, K. Xie, et al. "Polarization splitter based on dual core liquid crystal-filled  
298 holey fiber," *J. Appl. Phys.* **120**(11), 114501 (2016).

299 24.H. Wang, X. Yan, S. Li, et al. "Tunable surface plasmon resonance polarization beam splitter based on  
300 dual-core photonic crystal fiber with magnetic fluid," *Opt. Quant. Electron.* **49**(11), 368 (2017).

301 25.J. S. Wang, L. Pei, S. J. Weng, et al. "Ultrashort polarization beam splitter based on liquid-filled dual-  
302 core photonic crystal fiber," *Appl. Opt.* **57**(14), 3847-3852 (2018).

303 26.Q. Xu, W. L. Luo, K. Li, et al. "Design of polarization splitter via liquid and Ti infiltrated photonic  
304 crystal fiber," *Crystals* **9**(2), 103 (2019).

305 27.Y. W. Qu, J. H. Yuan, X. Zhou, et al. "Surface plasmon resonance-based silicon dual-core photonic  
306 crystal fiber polarization beam splitter at the mid-infrared spectral region," *J. Opt. Soc. Am. B* **37**(8),  
307 2221-2230 (2020).

308 28.Q. Liu, L. Xing, Z. X. Wu, et al. "High-sensitivity photonic crystal fiber force sensor based on Sagnac  
309 interferometer for weighing," *Opt. Laser Technol.* **123**, 105939 (2020).

310 29.I. H. Malitson, "Interspecimen comparison of the refractive index of fused silica," *J. Opt. Soc. Am. A*  
311 **55**(10), 1205-1209 (1965).

312 30.J. W. Fleming, "Dispersion in GeO<sub>2</sub>-SiO<sub>2</sub> glasses," *Appl. Opt.* **23**(24), 4486-4493 (1986).

313 31.A. Vial, A. S. Grimault, Macías D, et al. "Improved analytical fit of gold dispersion: Application to the  
314 modeling of extinction spectra with a finite-difference time-domain method," *Phys. Rev. B* **71**(8),  
315 085416 (2005).

316 32.K. Saitoh, Y. Sato, M. Koshiba, "Coupling characteristics of dual-core photonic crystal fiber  
317 couplers," *Opt. Express* **11**(24), 3188-3195 (2003).

318 33.M. Eisenmann, E. Weidel, "Single-mode fused biconical coupler optimized for polarization  
319 beamsplitting," *J. Lightw. Technol.* **9**(7), 853-858 (1991).

320 34.N. Florous, K Saitoh, M. Koshiba, "A novel approach for designing photonic crystal fiber splitters  
321 with polarization-independent propagation characteristics," *Opt. Express* **13**(19), 7365-7373 (2005).

322 35.Z. H. Zhang, Y. F. Shi, B. M. Bian, et al. "Dependence of leaky mode coupling on loss in photonic  
323 crystal fiber with hybrid cladding," *Opt. Express* **16**(3), 1915-1922 (2008).

324 36.A. Khaleque, E. G. Mironov, H. T. Hattori, "Analysis of the properties of a dual-core plasmonic  
325 photonic crystal fiber polarization splitter," *Appl. Phys. B* **121**(4), 523-532 (2015).

326 37.N. Gómez-Cardona, C. Jiménez-Durango, J. Usuga-Restrepo, et al. "Thermo-optically tunable  
327 polarization beam splitter based on selectively gold-filled dual-core photonic crystal fiber with  
328 integrated electrodes," *Opt. Quant. Electronics.* **53**(2), 1-15 (2021).

329 38.L. Chen, W. Zhang, Z. Zhang, et al. "Design for a single-polarization photonic crystal fiber  
330 wavelength splitter based on hybrid-surface plasmon resonance," *IEEE Photon J.* **6**(4), 1-9 (2014).

331 39.N. Chen, X. Zhang, X. Lu, et al. "Numerical investigation of a short polarization beam splitter based  
332 on dual-core photonic crystal fiber with As<sub>2</sub>S<sub>3</sub> layer," *Micromachines.* **11**(7), 706 (2020).

333 40.Z. K. Fan, S. G. Li, Y. Q. Fan, et al. "Designing analysis of the polarization beam splitter in two  
334 communication bands based on a gold-filled dual-core photonic crystal fiber," *Chin. Phys. B.* **23**(9),  
335 094212 (2014).

336 41.C. Jimenez-Durango, E. Reyes-Vera, N. Gomez-Cardona, “Ultra-short polarization beam splitter to  
337 operate in two communication bands based on a gold-filled dual-core photonic crystal fiber,” *J. Appl.*  
338 *Phys.* **Tu4A**, 16 (2018).

339 42.A. Khaleque, H. T. Hattori, “Ultra-broadband and compact polarization splitter based on gold filled  
340 dual-core photonic crystal fiber,” *J. Appl. Phys.* **118**(14), 143101 (2015).

341 **Ke Wang** is currently a graduate student in the state Key Laboratory of Information Photonics  
342 and Optical Communication department at Beijing University of Posts and Telecommunications.

343 **Yuwei Qu** is currently working toward the Ph.D. degree in electronic science and technology at  
344 Beijing University of Posts and Telecommunications (BUPT), Beijing, China. His research  
345 interests include photonic crystal fiber, surface plasmon resonance, and novel fiber devices.

346 **Jinhui Yuan** received the Ph.D. degree in physical electronics from Beijing University of Posts  
347 and Telecommunications (BUPT), Beijing, China, in 2011. He is currently a Professor at the  
348 Department of computer and communication engineering, University of Science and Technology  
349 Beijing (USTB). His current research interests include photonic crystal fibers, silicon waveguide,  
350 and optical fiber devices. He is the Senior Members of the IEEE and OSA.

351 **Shi Qiu** is currently working toward the Ph.D. degree in electronic science and technology at  
352 Beijing University of Posts and Telecommunications (BUPT), Beijing, China. His research  
353 interests include photonic crystal fiber sensors.

354 **Xian Zhou** received the Ph.D. degree in electromagnetic field and microwave technology from  
355 Beijing University of Posts & Telecommunications (BUPT), Beijing, China, in 2011. She is  
356 currently an Professor at the Department of Computer and Communication Engineering,  
357 University of Science & Technology Beijing (USTB). Her research interests are focused on  
358 highspeed optical communications, short reach communications, and digital signal nprocessing.

359 **Binbin Yan** received the B.S. and M.S. degrees from Beijing University of Posts and  
360 Telecommunications (BUPT), Beijing, China, in 2003 and 2005, respectively. In 2009, she  
361 received the Ph.D. degree from BUPT. Now she is with the BUPT as an Associate Professor. Her  
362 research interests include photonic devices and fiber optic sensing.

363 **Qiang Wu** received the B.S. and Ph.D. degrees from Beijing Normal University and Beijing  
364 University of Posts and Telecommunications, Beijing, China, in 1996 and 2004, respectively.  
365 From 2004 to 2006, he worked as a Senior Research Associate in City University of Hong Kong.  
366 From 2006 to 2008, he took up a Research Associate post in Heriot-Watt University, U.K. From  
367 2008 to 2014, he worked as a Stokes Lecturer at Photonics Research Centre, Dublin Institute of  
368 Technology, Ireland. He is currently an Associate Professor at Northumbria University, U.K. His  
369 research interests include photonics devices and fiber optic sensing.

370 **Bin Liu** received his B.S. and Ph.D. degree from Sun Yat-sen University, China. Dr. Liu is an  
371 associate Professor with Key Laboratory of Opto-Electronic Information Science and  
372 Technology of Jiangxi Province, Nanchang Hangkong University, Nanchang 330063, China. His  
373 research interests include optical fiber sensing and signal processing, nanofiber, microsphere  
374 sensors for bio-chemical sensing, nonlinear fiber optics, surface plasmon resonant.



375 **Kuiru Wang** received the B.S. and M.S. degrees from Beijing University of Posts and  
376 Telecommunications (BUPT), Beijing, China, in 1984 and 1990, respectively. In 2009, she  
377 received the Ph.D. degree from BUPT. Now she is with the BUPT as a Professor. Her current  
378 research interests include optical fiber communication and photonic devices.

379 **Xinzhu Sang** received the Ph.D. degree from Beijing University of Posts and  
380 Telecommunications (BUPT), Beijing, China, in 2005. Now he is with the BUPT as a professor.  
381 His current research interests include novel photonic devices, optical communication and optical  
382 interconnect. Prof. Sang is a senior Member of Chinese Institute of Communication, a committee  
383 of Holography and Optical information Processing, Chinese Optical Society, and a member of  
384 OSA.

385 **Chongxiu Yu** graduated from the Beijing University of Posts and Telecommunications (BUPT),  
386 Beijing, China, in 1969. Now she is with the BUPT as a Professor. Up to now she has published  
387 more than 300 papers. Her Research interests are the optical fiber communication, photonic  
388 switching, and optoelectronics technology and its applications. Prof. Yu is the Members of  
389 Chinese Institute of Communication, Committee of Fiber Optics and Integral Optics, and  
390 Chinese Optical Society.

#### 391 **Captions List**

392 **Fig. 1.** The cross-section of the proposed DC-PCF PBS.

393 **Fig. 2.** The effective refractive indices of the  $x$ -pol odd and even modes,  $y$ -pol odd and even  
394 modes,  $x$ -pol and  $y$ -pol first SPP modes, and zero SPP mode calculated as functions of  
395 wavelength.

396 **Fig. 3.** The mode field distributions of the  $x$ -pol odd mode,  $x$ -pol even mode,  $y$ -pol odd mode,  
397 and  $y$ -pol even mode calculated at wavelengths (a) 1.05  $\mu\text{m}$  and (b) 1.55  $\mu\text{m}$ .

398 **Fig. 4.** The relationships between the  $CL_x$ ,  $CL_y$ , and  $CLR$  and  $d$ .

399 **Fig. 5.** The relationships between the  $CL_x$ ,  $CL_y$ , and  $CLR$  and (a)  $A_1$  and (b)  $A_2$ .

400 **Fig. 6.** The relationships between the  $CL_x$ ,  $CL_y$ , and  $CLR$  and (a)  $d_{x1}$  and (b)  $d_{y1}$ .

401 **Fig. 7.** The relationships between the  $CL_x$ ,  $CL_y$ , and  $CLR$  and (a)  $d_{x2}$  and (b)  $d_{y2}$ .

402 **Fig. 8.** The relationships between the  $CL_x$ ,  $CL_y$ , and  $CLR$  and (a)  $d_{x3}$  and (b)  $d_{y3}$ .

403 **Fig. 9.** The relationships between the  $CL$  and  $CLR$  and wavelength, (a) without gold wires, and  
404 (b) with gold wires.

405 **Fig. 10.** The relationship between  $P_{\text{out}}$  of the  $x$ -pol and  $y$ -pol and propagation distance, and (b)  
406 the relationship between the  $ER$  and wavelength.

407 **Fig. 11.** The relationships between the  $ER$  and wavelength under  $\pm 1\%$  error of (a)  $d$ , (b)  $dx_1$ ,  $dy_1$   
408 (c)  $dx_2$ ,  $dy_2$ , and (d)  $dx_3$ ,  $dy_3$ .

409 **Table 1.** The comparisons between other proposed PCF PBS and this work.